

# Effect of Carbon Nanotubes on Solution Treatment Temperature and Dissolution Characteristics of Precipitates in Al Alloy Produced by High-Energy Milling and Hot Extrusion

N. S. Anas<sup>1,2</sup>  · S. B. Chandrasekhar<sup>1</sup> · R. K. Dash<sup>2</sup> · Tata N. Rao<sup>1</sup> · R. Vijay<sup>1</sup>

Received: 19 March 2019 / Accepted: 19 May 2019 / Published online: 6 June 2019  
© The Indian Institute of Metals - IIM 2019

**Abstract** The present study discusses the effect of CNT on the solution treatment temperature for Al alloy (AA), i.e. Al–4.4Cu–0.5 Mg, Al alloy–CNT (AC) and Al alloy–Ni-coated CNT (ANC) composites fabricated by mechanical milling and hot extrusion. Differential scanning calorimetry indicated that dispersion of CNT in Al alloy increased the dissolution temperature of  $\theta$  phase precipitates. X-ray diffraction (XRD) and scanning electron microscopy illustrated complete dissolution of  $\theta$  phase in both AA and AC samples when solution-treated at 520 °C, whereas ANC sample exhibited the same behaviour at 500 °C itself. XRD patterns of ANC sample revealed the presence of an additional intermetallic Al<sub>7</sub>Cu<sub>4</sub>Ni phase, which remains undissolved even after the solution treatment at 540 °C. Utilisation of Cu atoms to form Al<sub>7</sub>Cu<sub>4</sub>Ni phase resulted in significant reduction in size and number density of  $\theta$  phase in ANC. The hardness of AC and ANC samples was found to be higher compared to AA owing to dispersion strengthening by CNT and Al<sub>7</sub>Cu<sub>4</sub>Ni particles.

**Keywords** Aluminium matrix composites · Mechanical alloying · Solution treatment · Hardness

## 1 Introduction

Even though the age (precipitation) hardening of aluminium alloys was serendipitously discovered by Wilm in 1906 [1], the reason for an increase in hardness of Al–Cu alloy was not fully understood until transmission electron microscopy (TEM) and X-ray diffraction (XRD) techniques unravelled the presence of finer and uniformly distributed CuAl<sub>2</sub> precipitates [2]. These precipitates impede the movement of dislocations, thereby increasing the hardness and strength of Al alloy. The phenomenon of precipitation hardening stimulated tremendous interest amongst researchers to produce new and improved variants of Al alloys. This led to the development of Al alloy (Al–3.5Cu–0.5 Mg–0.5Mn) in the trade name ‘Duralumin’, which emerged as front-runner for automotive and aircraft components due to its outstanding specific strength [2]. Since then, the precipitation hardening mechanism is recognised as a major strengthening and design criterion in heat-treatable Al alloys (2xxx, 6xxx and 7xxx series) [3]. Precipitation hardening essentially involves three steps: (1) solution heat treatment, to obtain a single-phase ( $\alpha$ -Al) solid solution by the dissolution of alloying elements, (2) quenching, to obtain a supersaturated solid solution (SSSS) of solutes and vacancies at room temperature and (3) ageing treatment, to allow the precipitation of finer (nanometre-sized) and uniformly distributed second-phase coherent/semi-coherent ( $\theta''$  and  $\theta'$ ) particles with adequate volume fraction [2, 4]. Superior mechanical properties of precipitation-hardenable alloys are obtained only when the solution heat treatment is carried out appropriately to maximise the dissolution of solutes without compromising local or incipient melting [5, 6].

However, to increase the fuel efficiency and load carrying capacity of engines/vehicles, there is a need for a

✉ N. S. Anas  
anastzns@gmail.com

<sup>1</sup> International Advanced Research Centre for Powder Metallurgy and New Materials (ARCI), Balapur P O., Hyderabad 500 005, India

<sup>2</sup> School of Engineering Sciences and Technology, University of Hyderabad, Gachibowli, Hyderabad 500 046, India

**Table 1** Chemical composition (wt.%) of samples in this study

Sample	Description	Cu	Mg	CNT	Ni	Mn	Fe	Al
AA	Al alloy	4.4	0.5	–	–	–	0.17	Bal.
AC	Al alloy–CNT	4.4	0.5	1.5	–	–	0.16	Bal.
ANC	Al alloy–Ni-coated CNT	4.4	0.5	1.5	2.25	–	0.1	Bal.

further enhancement in strength, wear resistance and elevated homologous operating temperature capabilities of Al alloys that appear to be vital. These considerations lead to the development of composites based on Al and Al alloys with proper reinforcement materials such as hard particles, ceramics, fibres, or whiskers [7]. Although solution treatment temperature as well as mechanisms of heat-treatable wrought and cast Al alloys are well established [2, 3, 8, 9], similar details with regard to Al alloys and its composites produced through powder metallurgy (P/M) are comprehensively not available.

Recently, carbon nanotubes (CNTs) have emerged as efficient reinforcement materials in Al alloys due to the significantly extended strength and modulus limits [10, 11]. Even though CNT-reinforced Al matrix composites exhibit superior mechanical properties than the corresponding Al matrix due to dispersion and grain boundary strengthening mechanisms [12–15], these composites can not match their performance with the predicted levels. Based on the reported literature, it is understood that dispersion of CNT in Al/Al alloy increases the strength, but at the cost of its ductility. The reduction in ductility is due to weak interfacial bonding between Al matrix and CNT. In order to improve the interface bond, Cu- or Ni-coated CNTs are being used instead of bare CNTs [16–18]. It is reported that the Cu-coated CNT-reinforced Al alloy composites manufactured by milling and SPS exhibit more than 200% increase in strength as compared to wrought Al [17]. Enhancement in strength levels is also reported in Al (0–1 wt.%)–Cu-coated CNT composites produced by ultrasonic mixing, mechanical milling of powders followed by hot rolling [18]. However, it is observed that the dispersion of Cu-coated CNT in Al matrix does not appreciably improve the ductility [18]. In another work, Carvalho et al. produced Al–Si alloy–Ni-coated CNT composites by ball milling followed by pressing at 550 °C under vacuum [19, 20]. It is found that the rupture shear and yield strengths of Al–Si alloy–Ni-coated CNT composites increase by 12 and 27%, respectively, as compared to the base alloy without any reinforcement. The significant improvement in strength in the Al or Al alloy composites containing Ni-coated CNT is due to the formation of Al<sub>3</sub>Ni at the interface which facilitates effective load transfer to the matrix [17, 18, 20, 21].

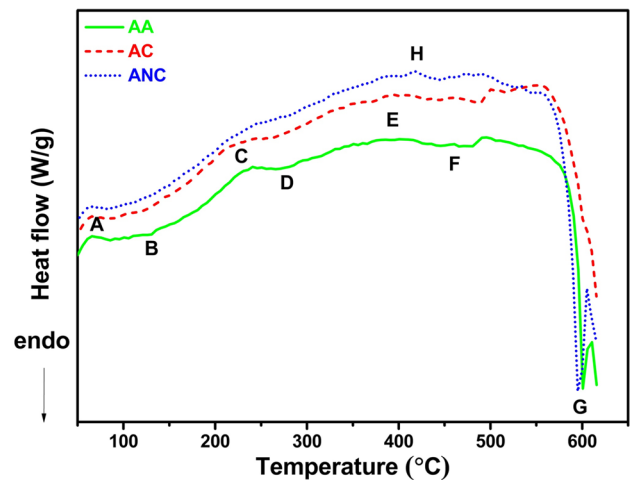


**Fig. 1** DSC thermograms of AA, AC and ANC composites solution-treated at 500 °C. The observed peaks correspond to: A—GP zone formation, B—GP zone dissolution, C— $\theta'$  phase formation, D— $\theta'$  phase dissolution, E— $\theta$  phase formation, F— $\theta$  phase dissolution, and G—incipient melting

Although CNT-reinforced Al matrix composites are well studied, there is no information about the influence of dispersion of CNT or Ni-coated CNT on the dissolution characteristics of precipitates in Al alloys. Therefore, this paper aims at the optimisation of solution treatment temperature and the resultant dissolution characteristics of Al alloy, Al alloy–CNT and Al alloy–Ni-coated CNT composites processed by mechanical milling and subsequent consolidation using hot extrusion.

## 2 Materials and Methods

Aluminium master alloy (Al–22Cu–0.5 Mg) was produced using high-energy planetary ball milling of commercial aluminium, copper and magnesium powders for 20 h [22]. The specifications of each of these powders and multi-walled carbon nanotubes (CNT) are given elsewhere [23]. Nickel-coated carbon nanotubes (Ni-coated CNT) of purity > 98% having an outer diameter of 50–80 nm and length 10–20  $\mu$ m procured from US Research Nanomaterials, Inc., USA, was also used in the present study. Al alloy, Al alloy–CNT and Al alloy–Ni-coated CNT composites (details of the composition are given in Table 1)

were prepared by blending the aluminium master alloy with the required quantities of Al, Mg, CNT and Ni-coated CNT powders. The blended powders were further subjected to mechanical milling in horizontal attrition mill for 4 h at 700 rpm under argon atmosphere using methanol (0.5 wt.%) as process control agent. Stainless steel balls of 5 mm diameter were used as milling media, and ball-to-powder weight ratio was maintained at 15:1 for all the samples. Milled powders were annealed at a temperature of 500 °C under a vacuum level of  $1 \times 10^{-4}$  mbar and subsequently filled in aluminium cans. The annealed powders were degassed at 300 °C under a vacuum level of  $1 \times 10^{-5}$  mbar and sealed. Upset forging of powder-filled cans was carried out at 500 °C, 350 MPa, and hot extrusion was carried out at 500 °C, 510 MPa, with an extrusion ratio of 16. Solution treatment was carried out on all the samples by heating at three different temperatures (500,

520 and 540 °C) for 2 h and water-quenched to room temperature. All the samples were stored in refrigerator to mitigate natural ageing and were exposed to ambient conditions only during characterisation. For ease of discussion, Al alloy, Al alloy–CNT and Al alloy–Ni-coated CNT composites are designated as AA, AC and ANC, respectively. Inductively coupled plasma optical emission spectroscopy technique was employed to analyse the chemical composition of the consolidated samples, and the details are given in Table 1.

Differential scanning calorimetry (DSC, STA 449 F3 Jupiter, Netzsch GmbH, Germany) was carried out on solution-treated samples from room temperature to 620 °C with a heating rate of 5 °C/min under argon atmosphere. XRD (Brukers AXS D8, Germany) analysis was performed using Cu-K $\alpha$  radiation ( $\lambda = 1.5406 \text{ \AA}$ ) with a step size of  $0.05^\circ 2\theta$  per sec. Lattice parameters of as-extruded and

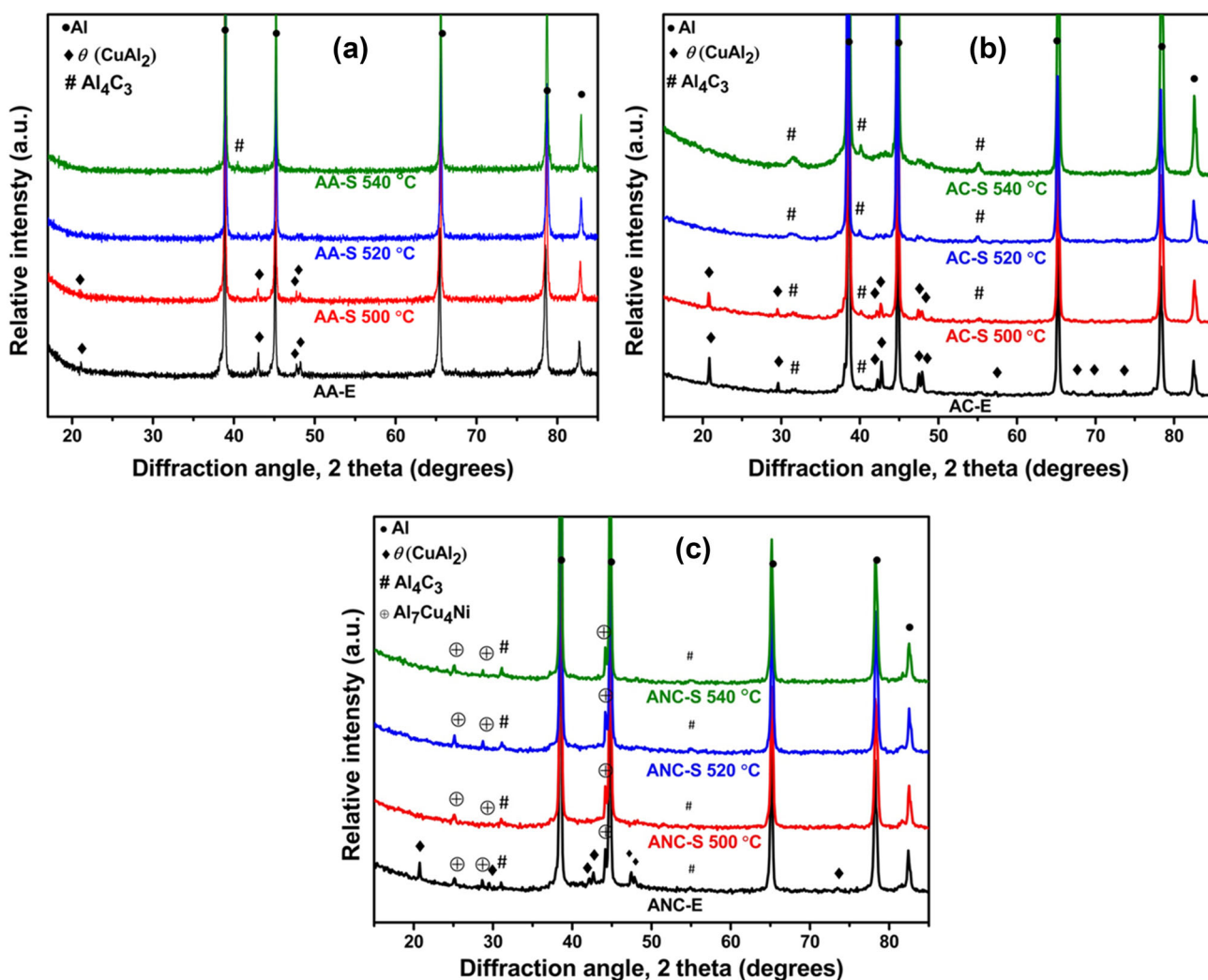


**Fig. 2** XRD patterns of: **a** AA, **b** AC and **c** ANC samples in as-extruded and solution-treated conditions. E represents as-extruded, and S 500 °C, S 520 °C and S 540 °C represent solution-treated conditions

solution-treated samples were estimated using Nelson–Riley extrapolation function, i.e.  $(\cos^2\alpha/\sin\alpha + \cos^2\alpha/\alpha)$ , where  $\alpha$  is the Bragg angle of diffraction [24, 25]. Samples were mounted and metallographically polished as per standard procedure and etched using modified Keller’s reagent. Scanning electron microscopy (SEM, Hitachi S4300 SE/N, Japan) was carried out on all the samples in as-extruded as well as solution-treated conditions to observe the changes in size and distribution of second-phase particles. The chemical composition of the precipitates was analysed using energy-dispersive spectroscopy (EDS) attached to SEM. The number density and particle size of undissolved  $\theta$  ( $\text{CuAl}_2$ ) particles were estimated using ‘Image analysis software’ from randomly taken SEM images. Samples for TEM were prepared by mechanical grinding to 100  $\mu\text{m}$  followed by dimpling up to 30  $\mu\text{m}$  and ion milling with argon at 4 kV. These samples were examined in a FEI

Tecnai G<sup>2</sup> TEM operated at an acceleration voltage of 200 kV. Matrix grain size of all the samples was measured from TEM dark-field images, and about 300 grains have been considered to estimate the average grain size of each sample. Measurement of hardness was carried out as per the ASTM E-384 standard using Vickers hardness (Leitz-112473, Germany) tester at a load of 5 N, and the average value of 15 measurements was reported.

### 3 Results and Discussion

#### 3.1 DSC Analysis of Solution-Treated Samples

The sequence of phase formation and its transformation in Al–Cu–Mg alloy during ageing treatment is: formation of GP/GPB zones  $>$   $\theta''/S'' >$   $\theta'/S' >$   $\theta/S$  phase, where  $\theta$  and

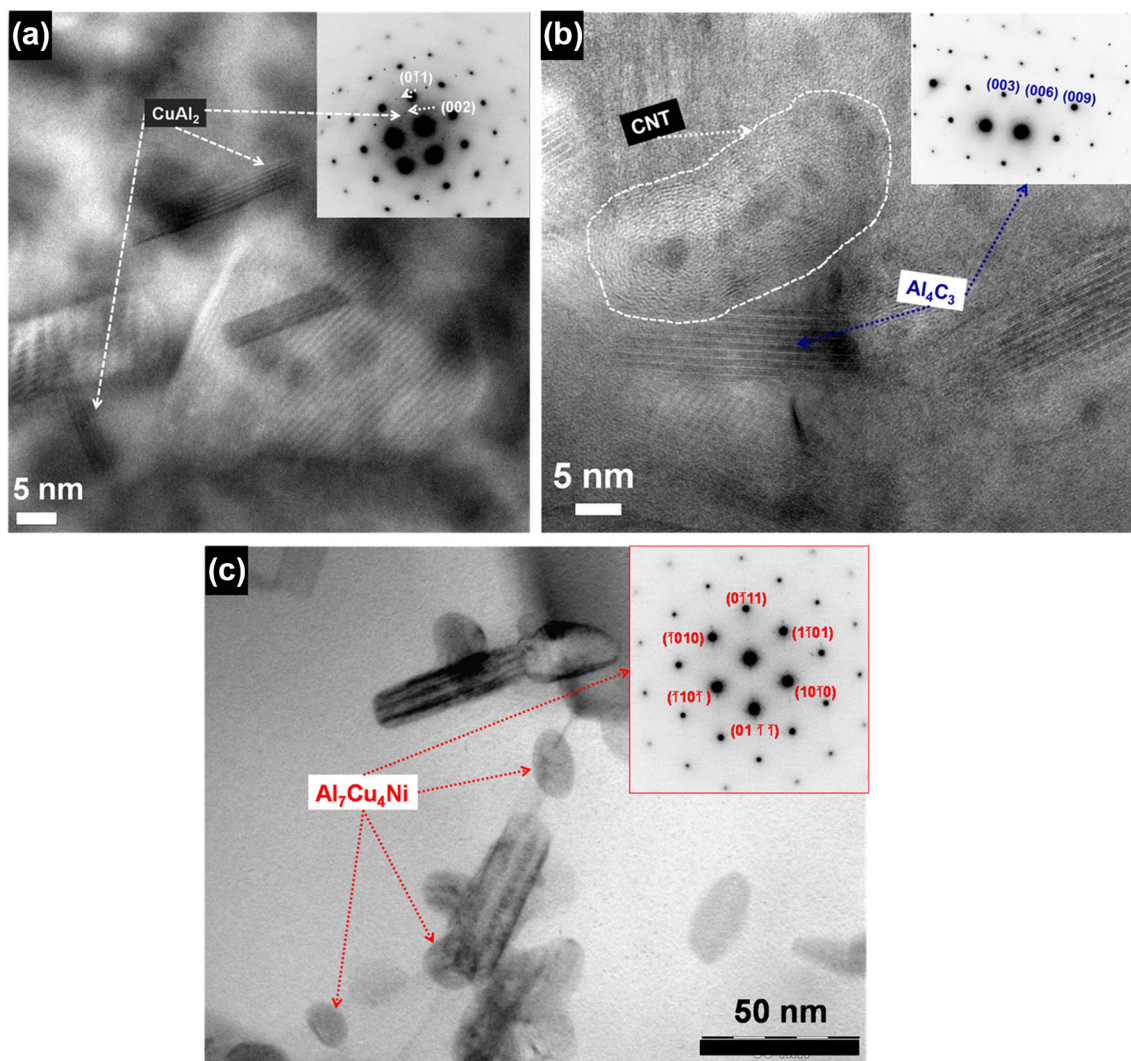


**Fig. 3** TEM micrographs showing nanocrystalline: **a**  $\text{CuAl}_2$ , **b**  $\text{Al}_4\text{C}_3$  and **c**  $\text{Al}_7\text{Cu}_4\text{Ni}$  particles. SAED patterns are shown as inset of corresponding figures



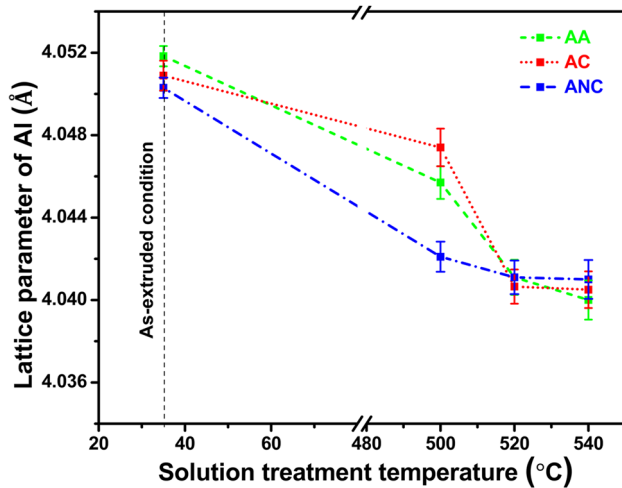


**Fig. 4** Variations in lattice parameter of Al matrix measured at room temperature for samples in as-extruded and solution-treated conditions

S ( $\text{Al}_2\text{CuMg}$ ) are the equilibrium phases, while the others are metastable phases [26–28]. In order to understand the formation and dissolution of various phases, DSC has been carried out on samples which are solution-treated at 500 °C and thermograms are shown in Fig. 1. In the case of AA sample, the exothermic region A in the temperature range of 50–85 °C and endothermic region B in the temperature range of 85–180 °C indicate the formation and dissolution of GP zones, respectively [29, 30]. This broad endothermic region includes the dissolution of undissolved  $\theta''$  also. The  $\theta'$  phase, which is the main strengthening phase, is found to form in the exothermic region C (180–225 °C). Subsequently,  $\theta'$  precipitates get dissolved in the endothermic region D (225–315 °C) [31]. Exothermic region E (315–430 °C) and endothermic region F (430–490 °C) correspond to the precipitation and dissolution of  $\theta$  phase, respectively [32]. The exothermic peak at E is observed to be broad, probably due to the presence of undissolved  $\theta$  phase even after solution treatment. An endothermic peak G at 601 °C is also observed due to the local or incipient melting of  $\theta$  phase. It is reported that the melting of  $\theta$  phase generally commences at 540 °C [6], and the same gets completed over a range of temperature of 540–610 °C [6, 33].

In the case of sample AC, GP zone formation and dissolution events fall in similar regions as that of AA sample. However, AC samples show a shift of both exothermic and endothermic peaks (regions C and D) towards the left indicating precipitation and dissolution of  $\theta'$  phase at lower temperatures when compared to AA sample. This is due to the generation of additional dislocations arising from the difference in thermal coefficient of expansion between Al alloy matrix and CNT [34], which provide more nucleation sites [35–37]. The complete dissolution of  $\theta$  phase in

sample AC has occurred slightly at higher temperature (505 °C) compared to AA. This shifting of thermal event from 490 °C in AA sample to 505 °C in AC may be attributed to the formation of  $\text{Al}_4\text{C}_3$  phase [38].

In contrast to AA and AC samples, a distinct exothermic peak (H) is observed at 420 °C in ANC samples due to the formation of an intermetallic  $\text{Al}_7\text{Cu}_4\text{Ni}$  phase, which is confirmed by XRD (Sect. 3.2). In order to have a clear idea about the chemistry of phase formation and its dissolution, a series of further confirmatory tests have been carried out using SEM and XRD for all the samples under as-extruded as well as solution-treated conditions.

### 3.2 Phase Formation in As-Extruded and Solution-Treated Samples

XRD patterns of AA, AC and ANC samples in as-extruded and solution-treated conditions are shown in Fig. 2a–c, respectively. All the samples exhibit aluminium peaks at the Bragg angle positions 38.454°, 44.708°, 65.0866°, 78.2306° and 82.415° corresponding to lattice planes (111), (200), (220), (311) and (222), respectively (ICDD# 04-012-7848), in both as-extruded and solution-treated conditions. As-extruded samples also show peaks corresponding to  $\theta$  phase (ICDD# 04-001-0923). However, the intensity of  $\theta$  peaks reduces after solution treatment at 500 °C and its absence at 520 and 540 °C indicates complete dissolution. However, a new phase,  $\text{Al}_4\text{C}_3$  (ICDD# 04-008-7186) is observed apart from  $\theta$  in AC and ANC samples under as-extruded condition itself as shown in Fig. 2b [39]. It is reported that during mechanical milling, the graphitic structure of CNT get damaged severely due to repetitive high kinetic impacts. These damaged ends undergo chemical reaction with Al to form  $\text{Al}_4\text{C}_3$  when exposed to high temperature during upset forging and hot extrusion [23, 38–40]. The fraction of  $\text{Al}_4\text{C}_3$  phase is observed to increase with solution treatment temperature. The presence of  $\text{Al}_7\text{Cu}_4\text{Ni}$  phase (ICDD# 04-007-2210) is the significant feature observed in ANC samples besides  $\theta$  and  $\text{Al}_4\text{C}_3$ , as shown in Fig. 2c. As per the Al–Cu–Ni ternary phase diagram, the intermetallic  $\text{Al}_7\text{Cu}_4\text{Ni}$  phase forms at higher Cu content [41]. Even though the Cu content is low, the formation of  $\text{Al}_7\text{Cu}_4\text{Ni}$  phase in the present study can be attributed to the preparation of ANC sample by mechanical milling, which is a well-known non-equilibrium process [42–44].  $\text{Al}_7\text{Cu}_4\text{Ni}$  phase is also identified in Al alloys with Cu composition similar to the one employed in this study [45–47]. ANC samples exhibit the complete dissolution of  $\theta$ , in contrast to other samples, when solution-treated at 500 °C itself. The lower dissolution temperature of  $\theta$  phase can be due to the utilisation of some quantity of Cu atoms towards the formation of  $\text{Al}_7\text{Cu}_4\text{Ni}$  in addition to  $\theta$  phase. TEM micrographs along with selected area electron

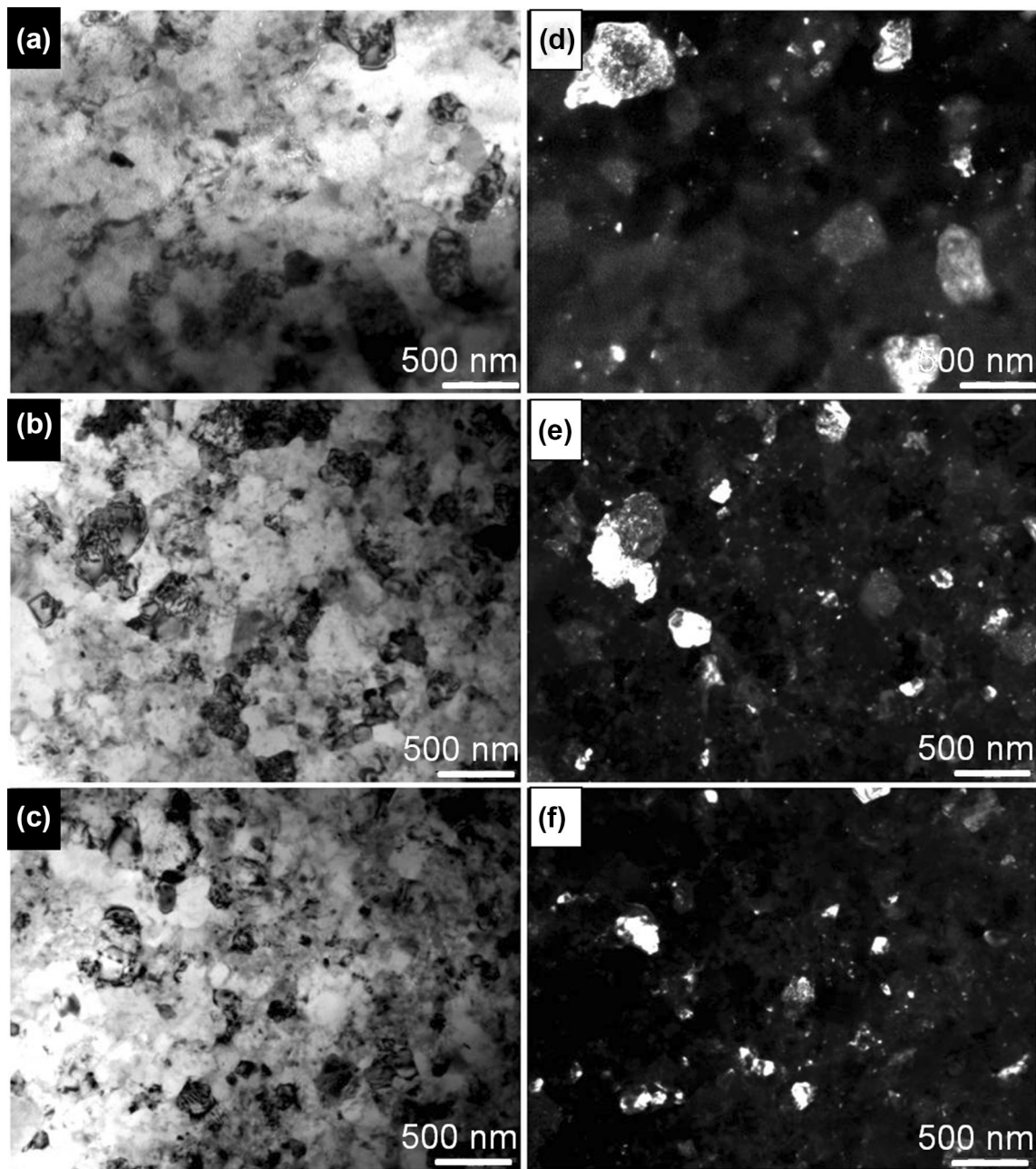


**Fig. 5** Microstructures of bulk samples after solution treatment: **a** AA, **b** AC and **c** ANC samples imaged using bright-field mode, and **d** AA, **e** AC and **f** ANC samples imaged using dark-field mode

diffraction (SAED) patterns, shown in Fig. 3a–c, also confirm the presence of  $\text{CuAl}_2$ ,  $\text{Al}_4\text{C}_3$  and  $\text{Al}_7\text{Cu}_4\text{Ni}$  particles in ANC sample. It may be noted that the AA sample exhibits  $\text{Al}_4\text{C}_3$  peak when the solution treatment temperature is more than  $500\text{ }^\circ\text{C}$  and this is due to the reaction of carbon from PCA with Al. Suryanarayana also reported that the presence of PCA can lead to the formation of carbides in the metal matrix [48].

### 3.3 Variations in Lattice Parameter with Composition and Solution Treatment

In order to understand the effect of solution treatment temperature on the dissolution behaviour of Cu and Mg in Al matrix, lattice parameter of Al is calculated from the maximum intensity peaks of XRD patterns of the respective samples and its variation as a function of solution treatment temperature is shown in Fig. 4. It can be observed that the lattice parameter of Al in all the samples,

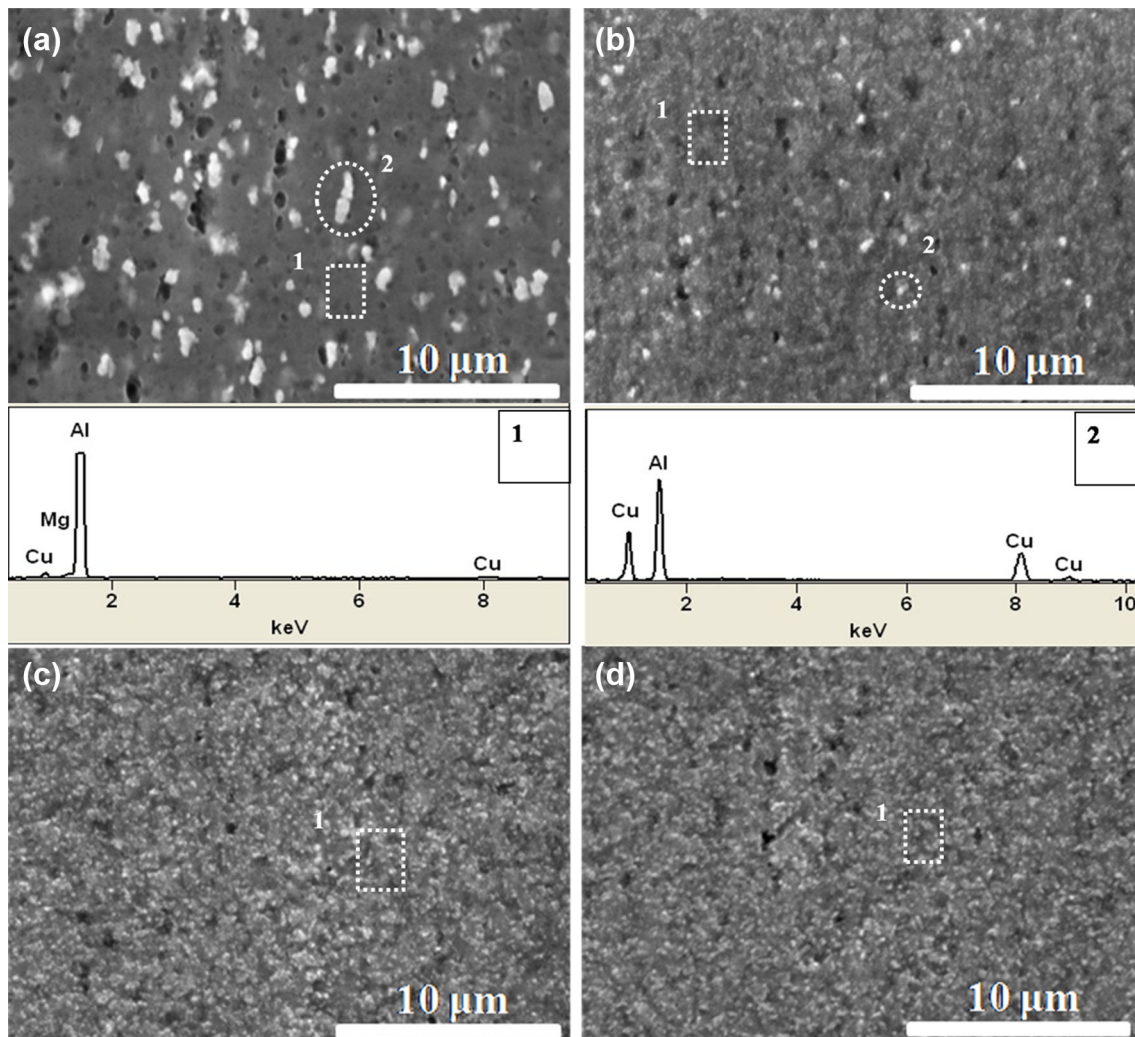


**Fig. 6** SEM images of AA samples in: **a** as-extruded and solution-treated at **b** 500 °C, **c** 520 °C and **d** 540 °C. EDS spectra of matrix (indicated as 1) and  $\text{CuAl}_2$  ( $\theta$ ) particles (indicated as 2) are also shown in the figure. All samples were deep-etched with modified Keller's reagent, 5000X

in general, decreases with increase in solution treatment temperature and reaches a steady state beyond 520 °C and the lattice parameter of Al in ANC sample is much lower at 500 °C as compared to AA and AC samples. Such a behaviour can be attributed to dissolution of Cu and Ni atoms in Al matrix of ANC at this temperature. It is reported that the expansion or contraction of Al lattice depends on the relative atomic size of solutes (lattice expansion for bigger atoms and contraction for smaller atoms) [25]. Al lattice (atomic radius = 1.429 Å) contracts when Cu (atomic radius = 1.276 Å) and Ni (atomic radius = 1.244 Å) are dissolved and it expands when Mg is dissolved (atomic radius = 1.598 Å) [49]. The resultant lattice parameter depends entirely on the percentage of dissolved Cu and Mg atoms [50, 51]. As the concentration of Mg is lower (0.57 at.%) when compared to Cu (1.92 at.%) in all the samples, the resultant lattice of Al will shrink. Therefore, upon increasing the temperature, the Cu

atoms diffuse from the precipitated  $\theta$  phase and form a solid solution that shrinks the Al lattice. It is observed that there is no significant reduction in lattice parameter when the solution treatments are carried out above 520 °C. This suggests that the dissolution of  $\theta$  has occurred at 520 °C in AA and AC samples and at 500 °C in ANC sample, which is also confirmed by the XRD results, as shown in Fig. 2a–c.

### 3.4 Microstructural Evaluation

Microstructures of bulk solution-treated samples obtained from TEM are shown in Fig. 5. Ultrafine grains of  $332 \pm 62$ ,  $220 \pm 83$  and  $172 \pm 66$  nm are observed in AA, AC and ANC samples, respectively. It is reported that during mechanical milling, the refinement of grains occurs due to generation and rearrangement of dislocations



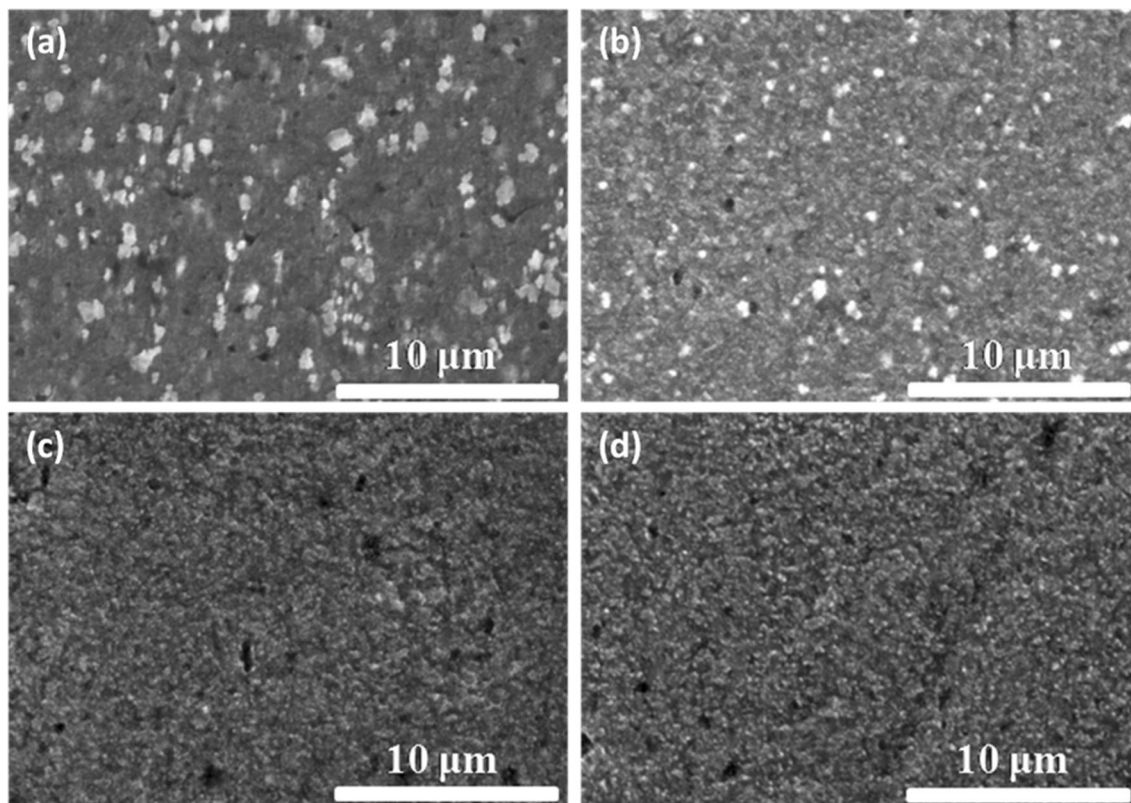


**Fig. 7** SEM images of AC samples in: **a** as-extruded and solution-treated at **b** 500 °C, **c** 520 °C and **d** 540 °C. Similar to Fig. 6, EDS analysis of the particles revealed the presence of  $\theta$  phase, and hence the spectrum is not given here. All samples were deep-etched with modified Keller's reagent, 5000X

[44, 48]. Also, the formation and subsequent dispersion of oxides into the matrix are expected during milling of Al and its alloys [43, 52], which pin the grain boundaries, thereby helps in retaining ultrafine grains even after solution treatment.

Figure 6a–d shows SEM micrographs of AA samples under as-extruded and solution-treated conditions. The chemical composition of matrix (grey background) and particles is given in EDS spectra 1 and 2, respectively. It is found that the particles distributed uniformly throughout the matrix are made up of a Cu-rich phase (Fig. 6a) and are confirmed to be  $\theta$  phase by XRD spectra (Fig. 2a). These particles are found to be slightly elongated along the extrusion direction. When solution-treated at 500 °C, the number density of  $\theta$  particles reduces substantially due to the dissolution of Cu in Al (Fig. 6b), while the shape of undissolved  $\theta$  particles is observed to be spherical. Complete dissolution of  $\theta$  is evident after solution treatment at 520 and 540 °C, as clear from Fig. 6c, d. These results are in complete agreement with that of XRD analysis of AA samples reported in the present study.

Morphologies of AC samples in as-extruded and solution-treated conditions are shown in Fig. 7a–d. Similar to

AA samples,  $\theta$  phase particles are also observed in AC samples and there is no significant change in the shape of particles. However, when solution-treated at 500 °C, AC sample exhibits only moderate dissolution of  $\theta$  particles as compared to AA. The remnant  $\theta$  particles present in AC are observed to be more in number and coarser than that of particles found in AA. AC sample also demonstrate complete dissolution of  $\theta$  after solution treatment at 520 and 540 °C.

Figure 8a–d shows the morphology of ANC samples in as-extruded and solution-treated conditions. EDS analysis indicates some particles corresponding to Al (Ni, Cu) phase (markings 2 in Fig. 8), in addition to  $\theta$  in the as-extruded condition. These Al (Ni, Cu) particles are confirmed to be an intermetallic  $\text{Al}_7\text{Cu}_4\text{Ni}$  phase, as shown in Fig. 2c. However,  $\text{Al}_7\text{Cu}_4\text{Ni}$  particles are found to be undissolved even after solution treatment at 520 and 540 °C. In contrast to other samples, complete dissolution of  $\theta$  occurs in ANC sample when solution-treated at 500 °C. SEM observations are in line with the results obtained from XRD (Fig. 2c) and lattice parameter measurements (Fig. 4).

In order to quantify the dissolution characteristics, the particle size and number density (ND) of undissolved  $\theta$



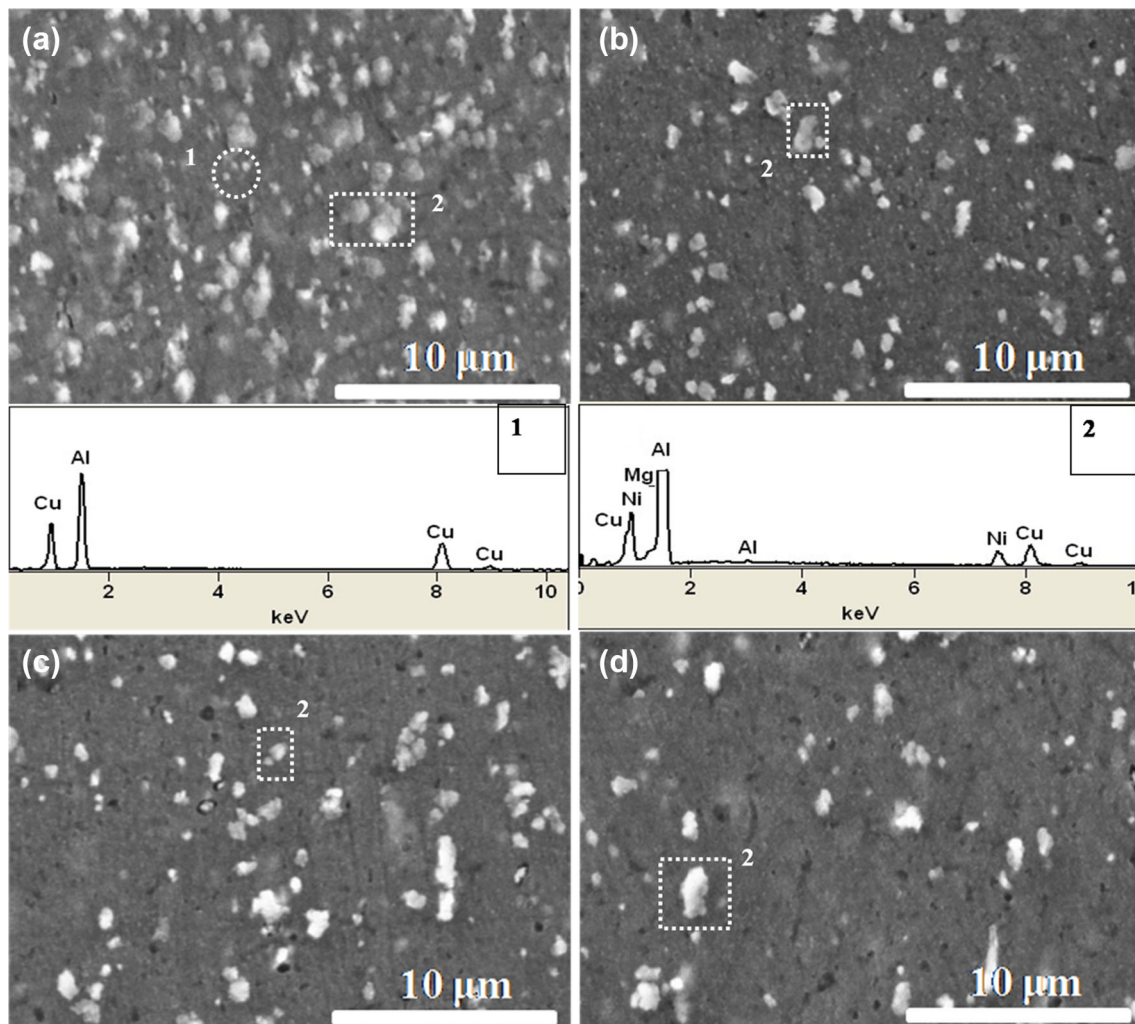


**Fig. 8** SEM images of ANC samples in: **a** as-extruded and solution-treated at **b** 500 °C, **c** 520 °C and **d** 540 °C. EDS spectra of particles corresponding to  $\theta$  (indicated as 1) and  $\text{Al}_7\text{Cu}_4\text{Ni}$  (indicated as 2) phases are also shown in the figure. All samples were deep-etched with modified Keller's reagent, 5000X

phase in all the samples have been measured from SEM images using image analysis software. SEM images are used for this estimation so that a larger area of observation is obtained than the TEM images. Moreover, nanoscale precipitates are assumed to dissolve during the solution treatments. It is found that the particle size and number density of undissolved  $\theta$  phase particles decreases from as-extruded to solution-treated condition at 500 °C as shown in Fig. 9a, b, respectively. Under as-extruded condition, the average size of  $\theta$  is found to be similar in both the samples, i.e.  $713 \pm 242$  nm and  $707 \pm 272$  nm for AA and AC, respectively. Even though the average particle size in both the samples is similar under as-extruded condition, the number density is found to be higher in AC sample. The size of remnant  $\theta$  after solution treatment at 500 °C is considerably reduced in AA ( $415 \pm 85$  nm) when compared to AC ( $516 \pm 102$  nm) but still the ND of particles

in the former case is found to be lesser. It is well known that the dissolution of phases in a matrix depends upon the diffusion coefficient of solute and solvent atoms, defects (grain boundaries, dislocations, vacancies, etc.) and the operating temperature [4]. Since AA and AC samples are solution-treated at the same temperature, the lone deciding factor is the availability of quenched-in vacancies for the diffusion to occur. Coarser remnant  $\theta$  particles are observed in AC due to the formation of an additional  $\text{Al}_4\text{C}_3$  phase, which must have consumed some amount of available vacancies [53]. In the case of ANC, only as-extruded condition is considered for the calculation of average particle size and ND of  $\theta$  phase, as  $\theta$  phase is found to dissolve at 500 °C itself (Figs. 2c, 8). ANC sample exhibits the least particle size ( $490 \pm 84$  nm) amongst all the samples in the present study. The lower dissolution temperature for  $\theta$

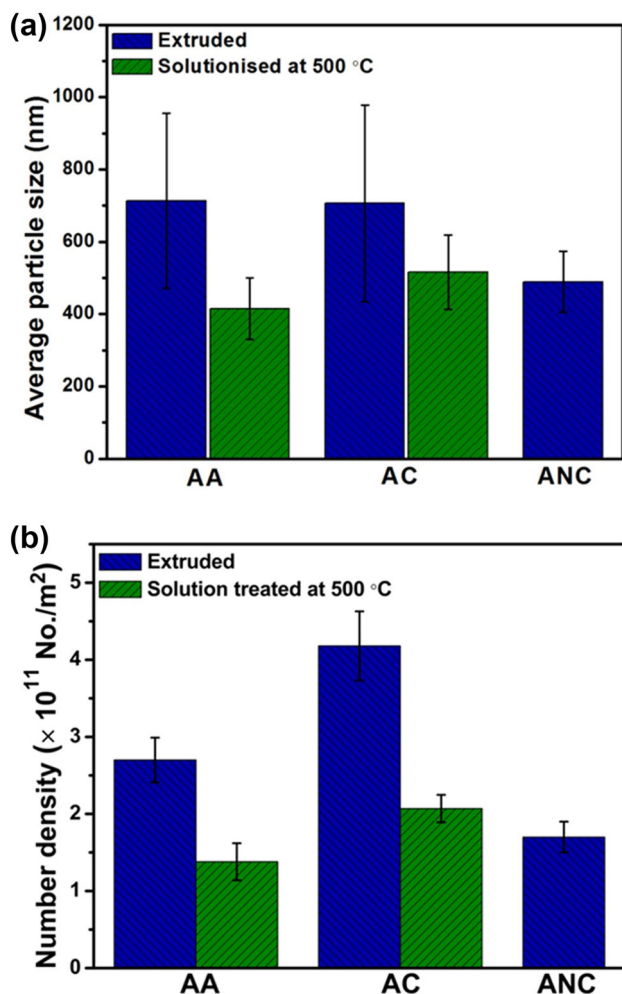


**Fig. 9** Variation in remnant  $\theta$ : **a** average particle size and **b** number density in AA and AC samples under as-extruded and 500 °C solution-treated conditions, and ANC sample in as-extruded condition

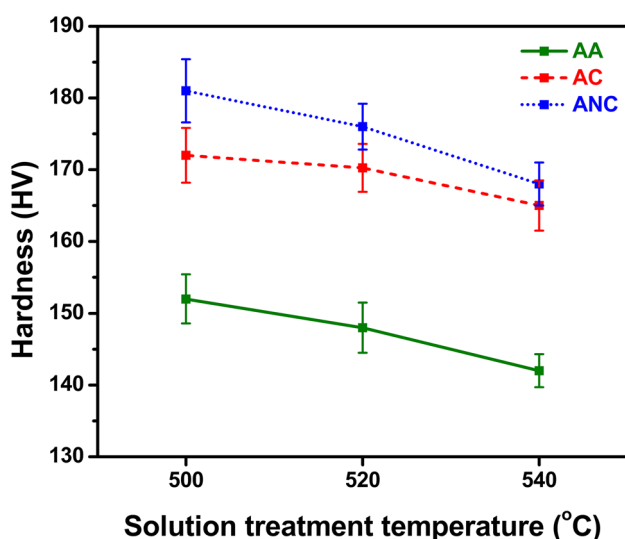


**Fig. 10** Variation in hardness for AA, AC and ANC samples with solution treatment temperature

particles exhibited by ANC can be rationalised based on their smaller size driving faster dissolution into the matrix.

### 3.5 Hardness of Solution-Treated Samples

Variation in hardness of all the samples with respect to different solution treatment temperatures are shown in Fig. 10. Hardness of the samples follows the order of AA < AC < ANC. It is to be noted that the hardness of AA sample is higher than that of wrought and cast AA2024 reported for same conditions of solution treatment [3]. This can be attributed to the presence of finer grains in AA sample that offer more grain boundaries as impediments to the moving dislocations, thus contributing to the increased hardness according to the Hall–Petch relationship [54, 55]. The observed insignificant reduction in hardness values even after the solution treatment of P/M-processed samples is due to the retention of ultrafine grains, as shown in Fig. 5. Amongst all the samples studied, AC and ANC exhibit higher hardness than AA owing to the dispersion of CNT [23, 56]. Marginally higher hardness observed in ANC as compared to that of AC sample may be attributed to the presence of Al<sub>7</sub>Cu<sub>4</sub>Ni particles.

## 4 Conclusions

Age-hardenable Al–4.4Cu–0.5 Mg Al alloy (AA), Al alloy–CNT (AC) and Al alloy–Ni-coated CNT composites (ANC) were produced by mechanical milling followed by hot extrusion. Different solution treatment temperatures (500, 520 and 540 °C) were carried out to optimise the dissolution of  $\theta$  (CuAl<sub>2</sub>) precipitates. The conclusions based on the research work carried out are given below:

1. DSC thermograms indicated the dissolution and incipient melting of  $\theta$  phase precipitates in the temperature range of 420–500 °C and 550–605 °C, respectively, in AA, AC and ANC samples.
2. Complete dissolution of  $\theta$  phase occurred in AA and AC samples when solution-treated at 520 °C. The same behaviour was observed at 500 °C itself for ANC sample, as lower fraction of Cu atoms was available due to the formation of an intermetallic Al<sub>7</sub>Cu<sub>4</sub>Ni phase.
3. The reduced lattice parameter of Al matrix after solution treatment at 520 °C in AA and AC samples, and 500 °C in ANC sample further confirmed the dissolution of  $\theta$  phase at the respective temperatures.
4. Particle size of  $\theta$  phase consistently decreased from as-extruded to solution-treated conditions for AA, AC and ANC samples

5. Without any exception, the hardness of AC and ANC samples were higher as compared to that of AA sample under all the conditions due to the presence of CNT, Al<sub>4</sub>C<sub>3</sub> and Al<sub>7</sub>Cu<sub>4</sub>Ni phases.

**Acknowledgements** The authors thank Nanomission project (No.: SR/NM/NS-102011G), Department of Science and Technology, Government of India, for the financial support to carry out this research. The technical assistance provided by Dr. Y. S. Rao, Mr. Balaji Padya, Mr. M. Ramakrishna and Mr. Ramesh Reddy is greatly acknowledged. The authors also thank Dr. L. Rama Krishna for his suggestions.

## References

- Wilm A, *Metallurgie* **8** (1911) 225.
- Polmear I, St. John D, Nie J-F, and Qian M, *The Light Metals—Light Alloys*, in: 5th ed., Butterworth-Heinemann, Boston (2017), pp 1–29.
- Davis J R, in *Aluminum and Aluminum Alloys*, ASM International Handbook Committee, (ed) Davis J R, ASM International, Materials Park, OH, USA (1993).
- Callister W D, *Fundamentals of Materials Science and Engineering*, 5th ed., Wiley, New York (2001).
- Starink M J, *Int Mater Rev* **49** (2004) 191.
- Samuel F H, *J Mater Sci* **33** (1998) 2283.
- Agarwal A, Bakshi S, and Lahiri D, *Carbon Nanotubes: Reinforced Metal Matrix Composites*, 1st ed., (ed) Meyyappan M, CRC Press, Boca Raton, FL (2011).
- Guo F-B, Zhu B-H, Jin L-B, Wang G-J, Yan H-W, Li Z-H, Zhang Y-A, and Xiong B-Q, *Rare Met* (2017) 1–8.
- Lv X, Guo E, Li Z, and Wang G, *Rare Met* **30** (2011) 664.
- Salvetat J-P, Kulik A J, Bonard J-M, Briggs G A D, Stöckli T, Méténier K, Bonnamy S, Béguin F, Burnham N A, and Forró L, *Adv Mater* **11** (1999) 161.
- Poole C P, and Owens F J, *Introduction to Nanotechnology*, 1st ed., Wiley, USA (2003).
- Pérez-Bustamante R, Pérez-Bustamante F, Estrada-Guel I, Licea-Jiménez L, Miki-Yoshida M, and Martínez-Sánchez R, *Mater Charact* **75** (2013) 13.
- Wu Y, Kim G Y, and Russell A M, *Mater Sci Eng A* **538** (2012) 164.
- Xu R, Tan Z, Fan G, Ji G, Xiong D-B, Guo Q, Su Y, Li Z, and Zhang D, *Compos Part A Appl Sci Manuf* **111** (2018) 1.
- Bakshi S R, and Agarwal A, *Carbon N Y* **49** (2011) 533.
- He C, Zhao N, Shi C, Du X, Li J, Li H, and Cui Q, *Adv Mater* **19** (2007) 1128.
- Jagannatham M, Sankaran S, and Haridoss P, *Mater Sci Eng. A* **638** (2015) 197.
- Maqbool A, Hussain M A, Khalid F A, Bakhsh N, Hussain A, and Kim M H, *Mater Charact* **86** (2013) 39.
- Carvalho O, Buciumeanu M, Soares D, Silva F S, and Miranda G, *J Mater Eng Perform* **24** (2015) 2535.
- Carvalho O, Buciumeanu M, Madeira S, Miranda G, and Silva F S, *Compos Part B Eng* **93** (2016) 229.
- Nam D H, Cha S I, Lim B K, Park H M, Han D S, and Hong S H, *Carbon N Y* **50** (2012) 2417.
- Anas N S, Ramakrishna M, Dash R K, Rao T N, and Vijay R, *Mater Sci Eng A* **751** (2019) 171.
- Anas N S, Dash R K, Rao T N, and Vijay R, *J Mater Eng Perform* **26** (2017) 3376.
- Nelson J B, and Riley D P, *Proc Phys Soc* **57** (1945) 160.
- Suryanarayana C, *X-ray Diffraction: A Practical Approach*, (ed) Norton M G, Springer, New York (1998).
- Hardy H K, and Heal T J, *Prog Met Phys* **5** (1954) 143.
- Ringer S P, and Hono K, *Mater Charact* **44** (2000) 101.
- Ringer S P, Sofyan B T, Prasad K S, and Quan G C, *Acta Mater* **56** (2008) 2147.
- Abis S, Massazza M, Mengucci P, and Riontino G, *Scr Mater* **45** (2001) 685.
- Jena A K, Gupta A K, and Chaturvedi M C, *Acta Metall* **37** (1989) 885.
- Wu Y P, Ye L Y, Jia Y Z, Liu L, and Zhang X M, *Trans Non-ferrous Met Soc China (Engl Ed)* **24** (2014) 3076.
- Shih H, and Huang J, *Metall Mater Trans A* **27A** (1996) 2479.
- Zlatianin B, Radonjic B, and Marinkovic Z, *Mater Sci Forum* **453–454** (2004) 193.
- Arsenault R J, and Shi N, *Mater Sci Eng* **81** (1986) 175.
- Weatherly G C, and Nicholson R B, *Philos Mag* **17** (1968) 801.
- García-Cordovilla C, and Louis E, *Metall Trans A* **15** (1984) 389.
- Ringer S P, Muddle B C, and Polmear I J, *Metall Mater Trans A* **26A** (1995) 1659.
- Kwon H, Estili M, Takagi K, Miyazaki T, and Kawasaki A, *Carbon N Y* **47** (2003) 570.
- Majid M, Majzoobi G H, Noozad G A, Reihani A, Mortazavi S Z, and Gorji M S, *Rare Met* **31** (2012) 372.
- He C N, Zhao N Q, Shi C S, and Song S Z, *J Alloys Compd* **487** (2009) 258.
- Mondolfo L F, *Aluminum Alloys: Structure and Properties*, 1st ed., Elsevier, Amsterdam (2013).
- Benjamin J S, and Volin T E, *Metall Trans* **5** (1974) 1929.
- Benjamin J S, and Bomford M J, *Metall Trans A* **8A** (1977) 1301.
- Gilman P S, and Benjamin J S, *Annu Rev Mater Sci* **13** (1998) 279.
- Li Y, Yang Y, Wu Y, Wang L, and Liu X, *Mater Sci Eng A* **527** (2010) 7132.
- Yang Y, Yu K, Li Y, Zhao D, and Liu X, *Mater Des* **33** (2012) 220.
- Chen C L, West G D, and Thomson R C, *Characterisation of Intermetallic Phases in Multicomponent Al–Si Casting Alloys for Engineering Applications*, in: Alum. Alloy. 2006—ICAA10, Trans Tech Publications, (2006), pp 359–364.
- Suryanarayana C, *Prog Mater Sci* **46** (2001) 1.
- Pauling L, *J Am Chem Soc* **69** (1947) 542.
- Axon H J, Phil D, and Hume-Rothery W, *Proc R Soc Lond A Math Phys Sci* **193** (1948) 1.
- Cocks F H, *J Mater Sci* **7** (1972) 771.
- Gilman P S, and Nix W D, *Metall Trans A* **12** (1981) 813.
- Ceresara S, and Fiorini P, *Powder Metall* **22** (1979) 1.
- Hall E O, *Proc Phys Soc Sect B* **64** (1951) 747.
- Petch N J, *J Iron Steel Inst* **174** (1953) 25.
- George R, Kashyap K T, Rahul R, and Yamdagni S, *Scr Mater* **53** (2005) 1159.

**Publisher's Note** Springer Nature remains neutral with regard to jurisdictional claims in published maps and institutional affiliations.